EMC effect in semi-inclusive deep-inelastic scattering processes

Baogui Lu
Department of Physics, Peking University, Beijing 100871, China

Bo-Qiang Ma*
CCAST (World Laboratory), P.O. Box 8730, Beijing 100080, China and Department of Physics, Peking University, Beijing 100871, China

(Received 10 April 2006; published 1 November 2006)

By considering the x-dependence of π^+, π^-, K^+, K^-, Λ, $\bar{\Lambda}$, p, $\bar{p}$ hadron productions in charged lepton semi-inclusive deep-inelastic scattering off nuclear target (using Fe as an example) and deuteron D target, we find that $(\bar{\Lambda}^A/\Lambda^A)/(\bar{\Lambda}^D/\Lambda^D)$ and $(\bar{p}^A/p^A)/(\bar{p}^A/p^A)$ are ideal to figure out the nuclear sea content, which is predicted to be different by different models accounting for the nuclear EMC effect.

DOI: 10.1103/PhysRevC.74.055202 PACS number(s): 13.60.Hb, 13.87.Fh, 25.30.Dh, 24.85.+p

I. INTRODUCTION

In 1982, the European Muon Collaboration (EMC) at CERN found that the structure function ratio of bound nucleon to free nucleon, in the form of $F_2^A(x, Q^2)/F_2^D(x, Q^2)$, is not consistent with the expectation by assuming that a nuclei is composed by almost free nucleons with Fermi motion correction taken into account [1,2], and such phenomenon was confirmed by E139 collaboration at SLAC [3]. This discovery, which is called the nuclear EMC effect, has received extensive attention by the nuclear and hadronic physics society. Many nuclear models, such as the pion excess model [4,5], the quark cluster model [6–8] and the rescaling model [6,9–12], have been proposed to explain the data, and all these models can qualitatively describe the data in the mediate x region. The inclusive deep inelastic scattering (DIS) data are expressed as $F_2^A(x, Q^2)/F_2^D(x, Q^2)$, which can be written in the naive parton model as:

$$\frac{F_2^A(x, Q^2)}{F_2^D(x, Q^2)} = \frac{\Sigma_i e_i^2[q_i(x, Q^2, A) + \bar{q}_i(x, Q^2, A)]}{\Sigma_i e_i^2[q_i(x, Q^2) + \bar{q}_i(x, Q^2)]}, \quad (1)$$

where e_i denotes the charge of the partons with flavor i, and $q(x, Q^2)$ is the parton distribution function of a nucleon. Figure 1 shows the $F_2^A(x, Q^2)/F_2^D(x, Q^2)$ results of the cluster model, the pion excess model and the rescaling model, respectively, at $Q^2 = 5\,\mathrm{GeV}^2$ in the mediate x region. All these models, as can be seen from Fig. 1, predict similar behavior of $F_2^A(x, Q^2)/F_2^D(x, Q^2)$ at mediate x region. However, the sea quark of the nuclei is differently described by the three models. In the cluster model, all sea quarks are enhanced. In the pion excess model, the sea quarks $\bar{u}$ and $\bar{d}$ are enhanced while the other quarks are reduced. However, in the rescaling model, all sea quarks are reduced in the nuclei compared with those in the free nucleon (Fig. 2).

The Fermilab experiment 772 [13] measured the dimuon yield in Drell-Yan process induced by 800 GeV proton off various nucleus and compared the data with the theoretical predictions of the three models accounting for the EMC effect [13]. The data were explained in Ref. [13] to favor a conclusion that the sea quark in the nuclei is not enhanced, by neglecting the energy loss effect of the incident quark, which is not precisely determined yet [14–16]. To avoid the uncertainties concerning the sea quarks in the nuclei by the dimuon yield in Drell-Yan process solely, the sea content can be also measured in other experiments. The purpose of this work is to show that the semi-inclusive hadron productions in charged lepton deep inelastic scattering are sensitive to the sea quark content of the nuclei. The pion, kaon, proton, and antiproton productions in the charged lepton semi-inclusive deep inelastic scattering off nuclei have been checked by the HERMES collaboration [17]. However, while the HERMES data, which are expressed as multiplicity ratios and also with z-dependence, are convenient to study the modification of the fragmentation functions in nuclear environment [17], they are not ideal to provide much information about the sea quarks of the nuclei. We will show that the $\bar{\Lambda}/\Lambda$ production, especially the x dependent behavior, is ideal to distinguish between different predictions on the sea content of the nuclei in the different models of the EMC effect.

II. NUCLEAR MODELS AND THE SEA QUARK DISTRIBUTIONS

The semi-inclusive hadron productions in charged lepton deep inelastic scattering can be related with the quark distribution functions as

$$\frac{d^3\sigma^h}{dxdydz} = \frac{4\pi\alpha s}{Q^4}(1 + (1 - y)^2) \sum_i e_i^2 \left[q_i(x, Q^2) \times D_{q_i}^h(z, Q^2) + \bar{q}_i(x, Q^2) D_{\bar{q}_i}^h(z, Q^2)\right], \quad (2)$$

where $q_i(x, Q^2)$ is the parton distribution for quarks with flavor i, and $D_{q_i}^h(z, Q^2)$ is the fragmentation function of quark q_i to hadron h. The formula is also applicable to the nuclei, with the parton distributions and fragmentation functions replaced by $q(x, Q^2) \to q(x, Q^2, A)$ and $D(z, Q^2) \to D(z, Q^2, A)$, respectively. The inclusive production itself can not offer enough information about the sea quark enhancement, while

*Electronic address: mabq@phy.pku.edu.cn

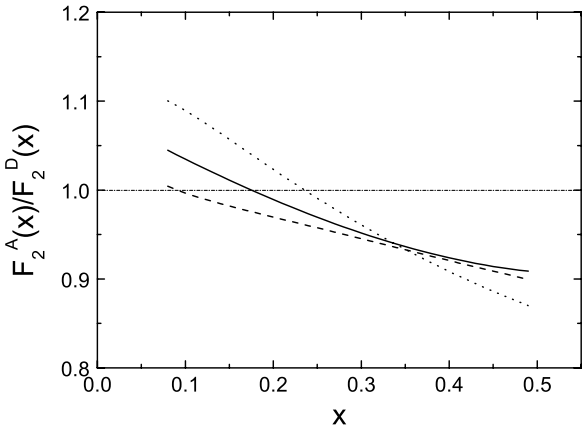

FIG. 1. Results of $F_2^A(x)/F_2^D(x)$ in three models at $Q^2 = 5\,\mathrm{GeV}^2$. The solid, dashed, and dotted curves are the results of the cluster model, the rescaling model, and the pion excess model, respectively. The target nuclei assumed here is Fe.

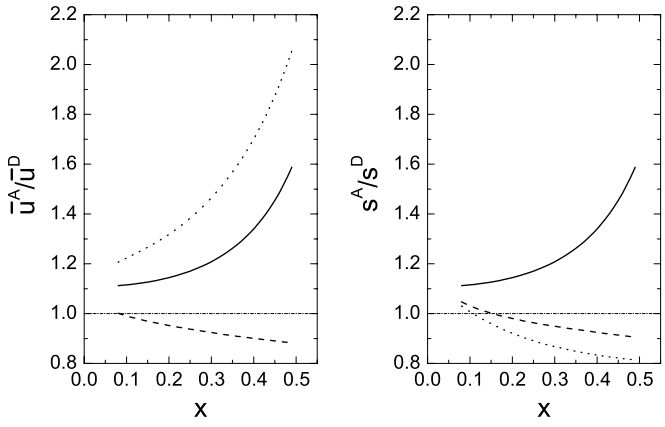

FIG. 2. $\bar{u}$ and s sea quark behaviors of various models. The solid, dashed, and dotted curves correspond to the predictions of the cluster model, the rescaling model, and the pion excess model, respectively. The parton distribution is calculated at $Q^2 = 5$ GeV^2. The target nuclei assumed here is Fe.

the ratio

$$\frac{d\sigma_A^h/dx}{d\sigma_D^h/dx} = \frac{\int_a^b dz \sum_i e_i^2 \left(q_i^A(x,Q^2) D_{q_i}^h(z,Q^2,A) + \bar{q}_i^A(x,Q^2) D_{\bar{q}_i}^h(z,Q^2,A)\right)}{\int_a^b dz \sum_i e_i^2 \left(q_i^D(x,Q^2) D_{q_i}^h(z,Q^2) + \bar{q}_i^D(x,Q^2) D_{\bar{q}_i}^h(z,Q^2)\right)}, \tag{3}$$

is useful to reveal the difference between the sea quark behavior in the nuclei and that in the nucleon.

In the following, we will consider the ratios $(d\sigma_A^h/dx)/(d\sigma_D^h/dx)$ for various hadrons. We use the pion excess model, the rescaling model and the pion excess model to calculate the sea quark content of the nuclei. For the sea quark distributions in the deuteron D, we use the result offered by the model itself [7] for the cluster model, and for the other two models we adopt the CTEQ5L parametrization [18] of parton distributions for free nucleons by considering the isospin symmetry between proton and neutron.

In the pion excess model, the quark distribution in the nuclei is modified by the extra pions caused by the interaction between the nucleons in nuclei [4]. The quark distribution of nuclei is

$$q_i^A(x) = \int_x^1 \frac{dy}{y} f_\pi^A(y) q_i^\pi\left(\frac{x}{y}\right) + \int_x^1 \frac{dy}{y} f_N^A(y) q_i^N\left(\frac{x}{y}\right), \tag{4}$$

in which $q_i^\pi(x)$ and $q_i^N(x)$ are the parton distributions in the free pion and in the free nucleon, respectively, and $f_\pi(y)$ is the probability to find extra pions in the nuclei [5]. For simplicity, we adopt the parametrization in a toy model [19], in which the proton is supposed to be partially in the nucleon-pion subsystem state and the parton distributions in the nucleon and in the pion are assumed to be the same as those in the free nucleon and in the free pion. Thus, the excess pion and the nucleon probabilities per nucleon are given as [19]

$$f_\pi^A(y) = \langle n_\pi \rangle \frac{\Gamma(a+b+2)}{\Gamma(a+1)\Gamma(b+1)} y^a (1-y)^b, \tag{5}$$

$$f_N^A(z) = (1 - \langle n_\pi \rangle)\delta(z-1) + f_\pi^A(1-z), \tag{6}$$

where $n_\pi = 0.22$, $a = 1$ and $b = 3$. The CTEQ5L [18] parametrization of the parton distribution of the nucleon and MRS [20] parametrization of the parton distribution of the pion are adopted to obtain $F_2^A(x)$ and the parton distribution of the nuclei.

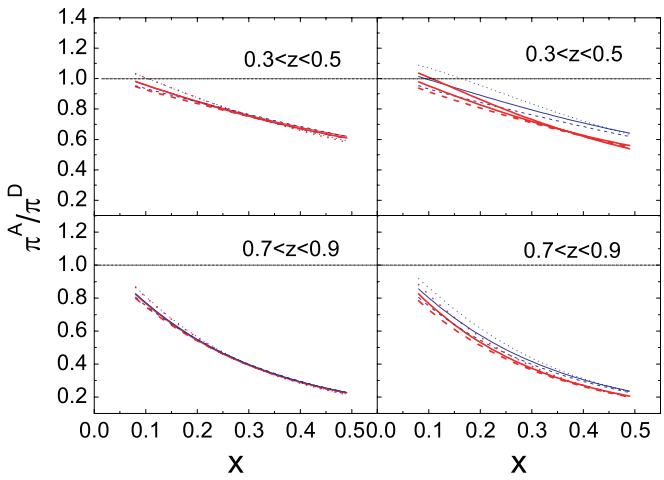

FIG. 3. (Color online) The production ratios of π^+, π^- at $Q^2 = 5$ GeV^2 in the region $0.7 < z < 0.9$ and $0.3 < z < 0.5$. The left two figures are the results of π^+ and the right are π^-. The upper two figures are in low z region and the lower two are in high z region. The solid, dashed, and dotted curves denote the results of the cluster model, the rescaling model, and the pion excess model, respectively. The thick curves denote the production with all quark fragmentation and the thin curves correspond to the results with only favored quark fragmentation. The left two are π^{+A}/π^{+D}, and the right two are π^{-A}/π^{-D} The target nuclei assumed here is Fe.

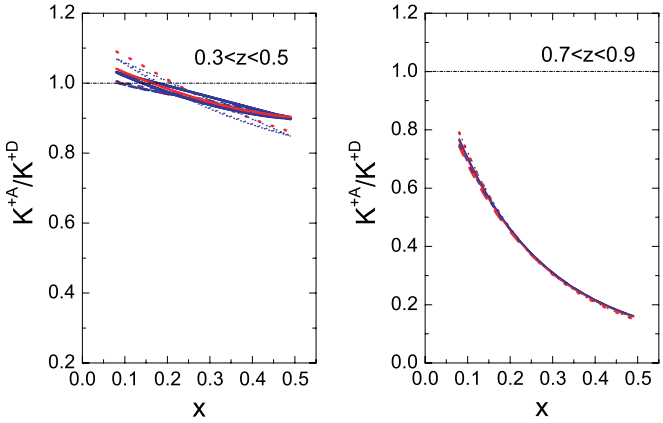

FIG. 4. (Color online) The production ratio of K^+ at $Q^2 = 5$ GeV^2 in the region $0.7 < z < 0.9$ and $0.3 < z < 0.5$. The left is the result in the low z region and the right is the result in the high z region. The solid, dashed, and dotted curves are the predictions of the cluster model, the rescaling model, and the pion excess model, respectively. The thick curves denote the production with all quark fragmentation and the thin curves correspond to the results when only favored quark fragmentation. The target nuclei assumed here is Fe.

In the quark cluster model, six or more quark cluster is supposed to exist in the nuclei to account for the EMC effect. For the sake of simplicity, only six quark cluster is considered here. $q(x)$ in a six-quark cluster can not be measured directly from experiment, but Carlson and Havens [7] estimated quark distribution $q(x)$ per nucleon in the six quark cluster based on QCD counting rules:

$$v_6(x) = N_v z^{(-1/2)}(1-z)^{10}, \tag{7}$$

$$\bar{u}_6(x) = (N_{\text{sea}}/4) z^{(-1)}(1-z)^{14}, \tag{8}$$

where $N_v = 1.3875$ and $N_{\text{sea}} = 0.2521$ are the coefficients to warrant momentum conservation and the quark number. In the six quark cluster, x, the variable defined by $Q^2/(2M_N\nu)$, equals to $2z$ because z is defined by $Q^2/(2M_6\nu)$ [7]. Therefore,

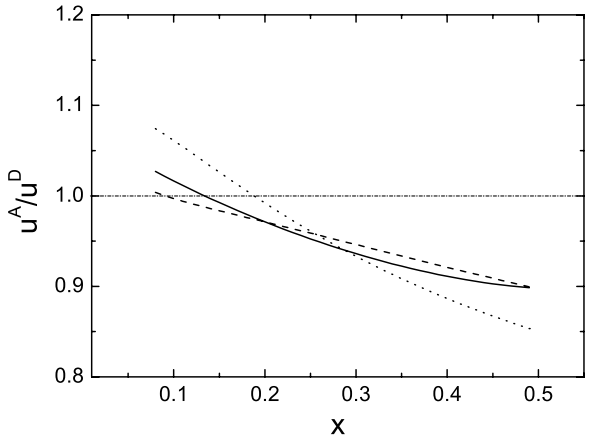

FIG. 5. The ratio $u^A(x)/u^D(x)$ of the three models at $Q^2 = 5$ GeV^2. The solid, dashed, and dotted curves are the predictions of the cluster model, the rescaling model, and the pion excess model respectively. The target nuclei assumed here is Fe.

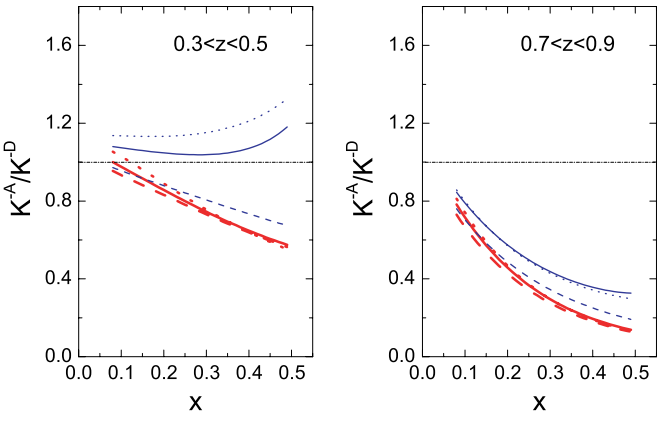

FIG. 6. (Color online) The production ratio of K^- at $Q^2 = 5$ GeV^2. The solid, dashed, and dotted curves are the predictions of the cluster model, the rescaling model, and the pion excess model, respectively. The left figure is the result in the region $0.3 < z < 0.5$ and the right is the result in the region $0.7 < z < 0.9$. The thick curves denote the total results including all quark fragmentation processes and the thin curves correspond to the results when only favored quark fragmentation processes. The target nuclei assumed here is Fe.

$q^A(x)$ and $F_2^A(x, Q^2)/F_2^N(x, Q^2)$ can be given as

$$q^A(x) = (1-f)q^N(x) + f q^6(x), \tag{9}$$

$$\frac{F_2^A(x,Q^2)}{F_2^N(x,Q^2)} = (1-f) + f\frac{F_2^6(x,Q^2)}{F_2^N(x,Q^2)}, \tag{10}$$

where f is the probability to find the six-quark cluster in the nuclei and is adjusted to fit the inclusive deep inelastic $e(\mu)$-A scattering data. Its value is given as 0.30 by Carlson and Havens [7].

For the rescaling model, the quark in the nuclear medium is considered to have different confinement size compared with that of the quark in the free nucleon. $q^A(x, Q^2)$ is related

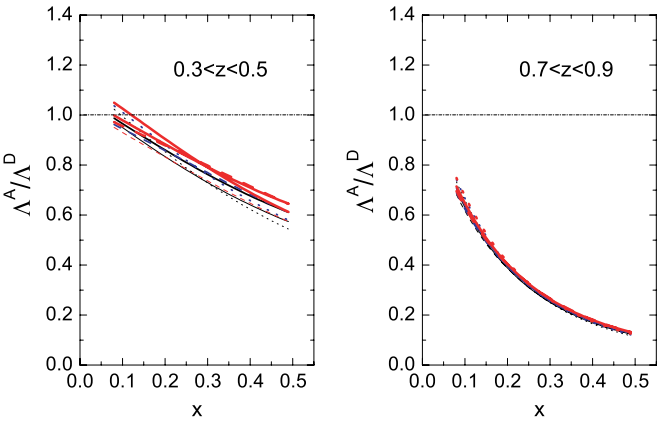

FIG. 7. (Color online) The ratio Λ^A/Λ^D at $Q^2 = 5$ GeV^2. The solid, dashed, and dotted curves are the predictions of the cluster model, the rescaling model, and the pion excess model, respectively. The left figure is the result in the region $0.3 < z < 0.5$ and the right is the result in the region $0.7 < z < 0.9$, with the thin, normal, and thick curves corresponding to the three options of the unfavored fragmentation (1), (2), (3), respectively. The target nuclei assumed here is Fe.

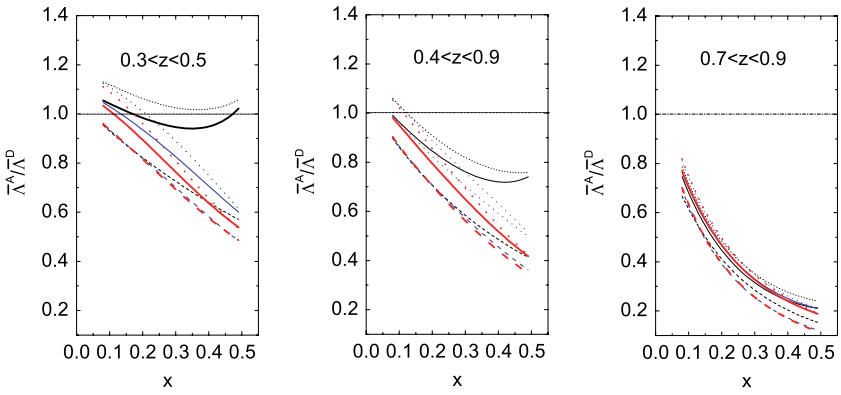

FIG. 8. (Color online) The production ratio of $\bar{\Lambda}^A/\bar{\Lambda}^D$ at $Q^2 = 5$ GeV^2. The solid, dashed and dotted curves are the predictions of the cluster model, the rescaling model and the pion excess model, respectively. The left figure is the result in the region $0.3 < z < 0.5$, the middle is the result in the region $0.4 < z < 0.9$ and the right is the result in the region $0.7 < z < 0.9$. The thin, normal, and thick curves correspond to the three options of the unfavored fragmentation (1), (2), (3), respectively. The target nuclei assumed here is Fe.

with $q^N(x, Q^2)$ (the parton distribution in the free nucleon) by the relation

$$q^A(x, Q^2) = q^N(x, \xi(Q^2)Q^2), \tag{11}$$

where $\xi(Q^2)$ varies with A and Q^2. ξ equals to 1.83 [11] while $Q^2 = 5$ GeV^2 and A = 56 (Fe). For $q^N(x, Q^2)$, the parton distribution per nucleon, CTEQ5L parametrization [18] is adopted.

Given the above analysis, $F_2^A(x, Q^2)/F_2^D(x, Q^2)$ and sea quark enhancement are checked in Figs. 1 and 2.

III. FRAGMENTATION FUNCTION AND PARTON ENERGY LOSS MODEL

Due to the nonperturbative nature of the fragmentation process, the fragmentation function can not be calculated from first principle, thus models are used to obtain the fragmentation function. Experimentally, the process of $e^+ + e^- \to h + X$ can offer much information about the fragmentation [21].

Based on the experimental data and theoretical analysis, Kretzer [22] gave a parametrization of the fragmentation in the form

$$D_a^h(x, Q_0^2) = Nx^\alpha(1-x)^\beta, \tag{12}$$

where N, α, and β are the constants chosen to fit the experimental data. For specified hadron, α, which determines the low z region behavior of the fragmentation function, is the same for all light flavor quarks while β, related with the high z region behavior of the fragmentation function, is different for various quarks. Therefore, in low z region, all quark fragmentation functions have the same shape, and in the large z region, the favored quark fragmentation function is larger than the unfavored quark fragmentation function. In addition, because of the strange dominance at large x for s in K^-, the fragmentation function such as $s \to K^-$ is larger than that of $\bar{u} \to K^-$.

As for $\Lambda, \bar{\Lambda}, p, \bar{p}$, there exists a phenomenological parametrization [23] of their fragmentation functions based on the assumption that the fragmentation function of quark q to hadron h is proportional to the q quark distribution in the hadron h:

$$D_q^h(z) \propto q^h(z). \tag{13}$$

In general, the fragmentation functions can be written as

$$D_V^h(z) = C_V(z)z^\alpha q_V^h(z), \tag{14}$$

$$D_S^h(z) = C_S(z)z^\alpha q_S^h(z), \tag{15}$$

where $D_S^h(z)$ means unfavored fragmentation function. There are three options for the favored and unfavored quark fragmentations: (1) $C_V = 1$ and $C_S = 0$ for $\alpha = 0$; (2) $C_V = 1$ and $C_S = 1$ for $\alpha = 0.5$; (3) $C_V = 1$ and $C_S = 3$ for $\alpha = 1$. The parton distributions of Λ and $\bar{\Lambda}$ are essential to get the fragmentation functions of quark to Λ and $\bar{\Lambda}$. Based on the fact that there is no direct parton distribution of Λ and $\bar{\Lambda}$, SU(3) symmetry between the proton and the Λ is adopted to get the parton distribution in Λ [23]. Although there are three models, SU(3) symmetry model, quark-diquark model and pQCD based analysis, the difference of the fragmentation functions will not affect the qualitative predictions by the fact that only the flavor structure of the parton distributions of the proton are different in the three models in the high x region [24].

The common feature of the above parameterizations of fragmentation functions is that the favored quark fragmentation is larger than the unfavored quark fragmentation in the large

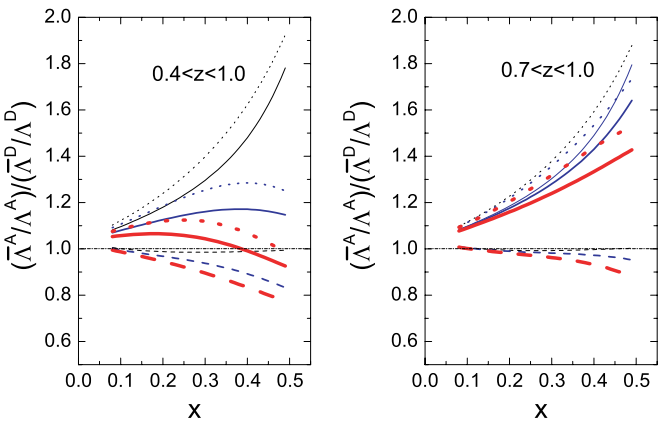

FIG. 9. (Color online) The production ratio of $(\bar{\Lambda}^A/\Lambda^A)/(\bar{\Lambda}^D/\Lambda^D)$ at $Q^2 = 5$ GeV^2, calculated in $0.7 < z < 1.0$ and $0.4 < z < 1.0$. The solid, dashed, and dotted curves are the predictions of the cluster model, the rescaling model, and the pion excess model, respectively. The thin, normal, and thick curves correspond to the three options of the fragmentation (1), (2), (3), respectively. The target nuclei assumed here is Fe.

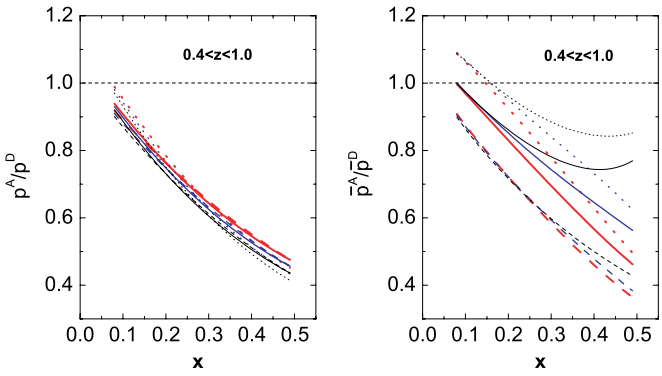

FIG. 10. (Color online) The ratio $\bar{p}^A/\bar{p}^D$(right) and p^A/p^D(left) at $Q^2 = 5$ GeV^2. The solid, dashed, and dotted curves are the predictions of the cluster model, the rescaling model, and the pion excess model, respectively. Thin, normal, and thick curves correspond to the three options of the unfavored fragmentation (1), (2), (3), respectively. The target nuclei assumed here is Fe.

z region. Thus the favored quark fragmentation process is able to obtain sea quark information of the nuclei if the produced hadron is from the favored fragmentation of sea quarks in the nuclei. Then the hadron events of produced particles in the large z region can be chosen to get the x dependence of the production ratio, in which the unfavored fragmentation contribution from the valence quark can be largely suppressed.

Fragmentation function in the nuclei is important for producing the hadron production from the nuclei. HERMES collaboration has measured the hadron production from the nuclei and found that the production is reduced compared with that from the free nucleon [17], and many effects such as nuclear absorption [25], parton energy loss [26,27], gluon bremsstrahlung [28] and partial deconfinement [10–12,29] have been developed to account for the data. In this paper, the parton energy loss model is adopted to get the fragmentation function in the nuclei.

In Refs. [26,27], the modification of the fragmentation function is caused by the interaction between the hard quark and the debris of the nuclei. Given that the original parton energy loss model is complicated to apply in the real process, an effective model suggested in Ref. [30] is used in Ref. [31] to get the modification of the fragmentation function. In effective parton energy loss model, modified fragmentation function is expressed in the form

$$zD_q^h(z, Q^2, A) = \int_0^{(\nu - E_h)} d\epsilon D(\epsilon, \nu) z^* D_q^h(z^*, Q^2), \quad (16)$$

where $E_h = \mu - \epsilon$. E_h is the measured hadron energy and ϵ is the energy loss of the hard quark going through the nuclei. z^* is the rescaled momentum fraction caused by the quark energy shift in presence of QCD medium:

$$z^* = \frac{E_h}{1 - \left(\frac{\epsilon}{\nu}\right)}. \quad (17)$$

$D(\epsilon, Q^2)$, the probability for a quark with energy $E = \nu$ to lose energy ϵ, is parametrized by Arleo [32]:

$$D(\epsilon) = \frac{1}{\sqrt{2\pi}\sigma\epsilon} \exp\left[-\frac{(\log(\epsilon/\omega_c) - \mu)^2}{2\sigma^2}\right], \quad (18)$$

where μ, σ are two parameters with $\sigma = 0.73$ and $\mu = -1.5$, as the energy of the quark, which has absorbed the virtual photon, is much higher than the energy loss when it passes through the nuclei environment. And ω_c is the relevant scale of the typical gluon energy and denotes the energy loss scale of the hard quark,

$$\omega_c = \tfrac{1}{2}\hat{q}L^2. \quad (19)$$

Although $\hat{q}$ is not precisely determined yet, in the next section we will show that the result is not sensitive on $\hat{q}$ when Q^2 is large enough. Here we set $\hat{q} = 0.72$ GeV/fm^2 and $L = 3/4R$, where R is the nuclear radius [31].

From another point of view, the modification of the fragmentation function in the parton energy loss model is from

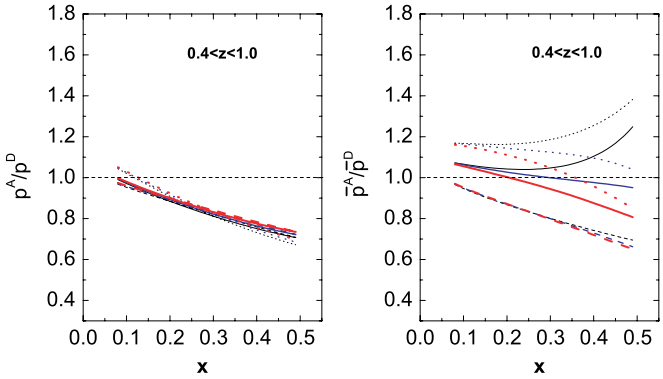

FIG. 11. (Color online) The ratio $\bar{p}^A/\bar{p}^D$(right) and p^A/p^D(left) at $Q^2 = 5$ GeV^2 with $\hat{q} = 0.25$ GeV/fm^2. The solid, dashed, and dotted curves are the predictions of the cluster model, the rescaling model, and the pion excess model, respectively. Thin, normal, and thick curves correspond to the three options of the unfavored fragmentation (1), (2), (3), respectively. The target nuclei assumed here is Fe.

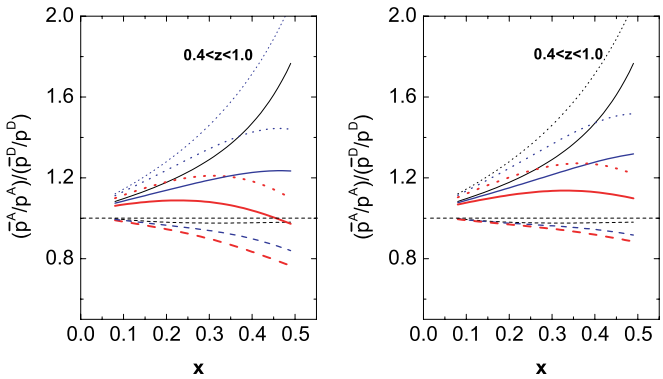

FIG. 12. (Color online) The ratio $(\bar{p}^A/p^A)/(\bar{p}^A/p^A)$ at $Q^2 = 5$ GeV^2 with $\hat{q} = 0.72$ GeV/fm^2 (left) and $\hat{q} = 0.25$ GeV/fm^2(right). The solid, dashed, and dotted curves are the predictions of the cluster model, the rescaling model, and the pion excess model, respectively. Thin, normal, and thick curves correspond to the three options of the unfavored fragmentation (1), (2), (3), respectively. The target nuclei assumed here is Fe.

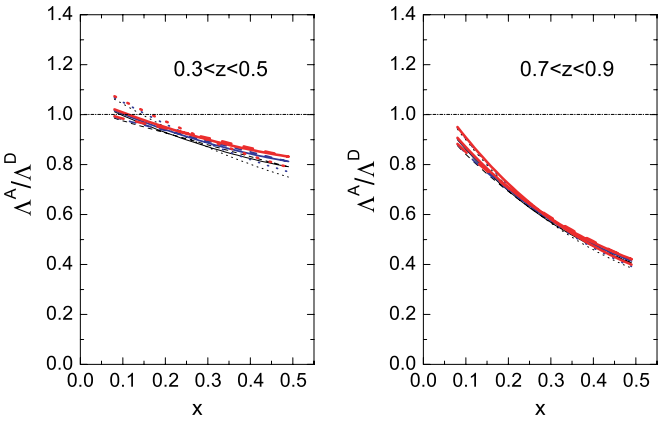

FIG. 13. (Color online) The ratio Λ^A/Λ^D at $Q^2 = 5$ GeV^2 with $\hat{q} = 0.25$ GeV/fm^2. The solid, dashed, and dotted curves are the predictions of the cluster model, the rescaling model, and the pion excess model, respectively. The left figure is the result in the region $0.3 < z < 0.5$ and the right is the result in the region $0.7 < z < 0.9$, with the thin, normal, and thick curves corresponding to the three options of the unfavored fragmentation (1), (2), (3), respectively. The target nuclei assumed here is Fe.

assumption. Its conformation with the theoretical framework of factorization and renormalization is not fully justified, as the definition of the fragmentation functions are vacuum matrix elements with no relation to the target material. As we will find, the qualitative conclusion of our paper on the ratio $(\bar{\Lambda}^A/\Lambda^A)/(\bar{\Lambda}^D/\Lambda^D)$ will not be influenced by including the modification of the fragmentation function in the nuclear environment. In order to get rid of the nuclear absorption or the energy loss process, it would be fine to consider hadron production at larger energy (say larger than 20 GeV), hence at higher virtuality, where we know from the present HERMES data that these two effects prove negligible.

IV. RESULTS

Figures 3 and 4 present the results of $\pi^+(u\bar{d})$, $\pi^-(\bar{u}d)$ and K^+, respectively. They show that there is no large difference between various model predictions in the large z region and in the low z region, no matter by including the favored quark fragmentation process only or by including all favored and unfavored fragmentation processes. The reason is that $\pi^+(u\bar{d})$, $\pi^-(\bar{u}d)$ and K^+ are contributed mainly by the favored fragmentation processes $u \to \pi^+$, $d \to \pi^-$ and $u \to K^+$ because that the valence quarks u and d are predominant over the sea quarks in the mediate x region and that production of those hadrons are dominated by the behavior of the valence quark in the nuclei (Fig. 5).

When focused on K^-, the result with only favored quark fragmentation functions is different from that when all fragmentation processes are considered (Fig. 6), which indicates that the unfavored quark fragmentation function, u and d to K^-, can not be neglected both at low and high z region for the predominance of the valence quarks in the x region we considered. In the high z region, due to parton energy loss, the K^- is largely suppressed and we can hardly see any difference in the three model predictions with all fragmentation processes being considered.

Λ and $\bar{\Lambda}$ production ratios in different z regions are examined and the results are plotted in Figs. 7 and 8. For the same reason as K^+, three models predict almost the same x-dependence of Λ^A/Λ^D. From Fig. 8, difference are generated among various model predictions on the x-dependence of $\bar{\Lambda}^A/\bar{\Lambda}^D$, and the these difference are not sensitive to the three options of the fragmentation functions [23]. The reason is that the dominant production of $\bar{\Lambda}$ is through the favored fragmentation of antiquarks inside the targets, so that the x-dependence of the production ratio is sensitive to the sea quark behaviors of the nuclei. But in the large z region, due to the parton energy loss effect, the large difference between three models do not manifest themselves significantly as expected. The reason is, at large z region, the fragmentation function is largely modified by the parton energy loss. And such a phenomenon also happens on Λ^A/Λ^D. Figure 8 shows that $\bar{\Lambda}^A/\bar{\Lambda}^D$ is not an ideal variable to figure out the nuclear sea quark content by including the modification of the fragmentation function in the nuclear environment. Fortunately, largely difference between three models appears for the quantity $(\bar{\Lambda}^A/\Lambda^A)/(\bar{\Lambda}^D/\Lambda^D)$, which is more accessible in experiment than $\bar{\Lambda}^A/\bar{\Lambda}^D$. When the integral upper limit is fixed with unity and the lower limit varies from 0.4 to 0.7, $(\bar{\Lambda}^A/\Lambda^A)/(\bar{\Lambda}^D/\Lambda^D)$ is still model dependent (Fig. 9). Thus it is plausible to conclude that $(\bar{\Lambda}^A/\Lambda^A)/(\bar{\Lambda}^D/\Lambda^D)$ can offer information about the sea content of the nuclei.

Similar to $\bar{\Lambda}^A/\bar{\Lambda}^D$, the antiproton and proton production ratio $(\bar{p}^A)/(\bar{p}^D)$ can not offer much information while

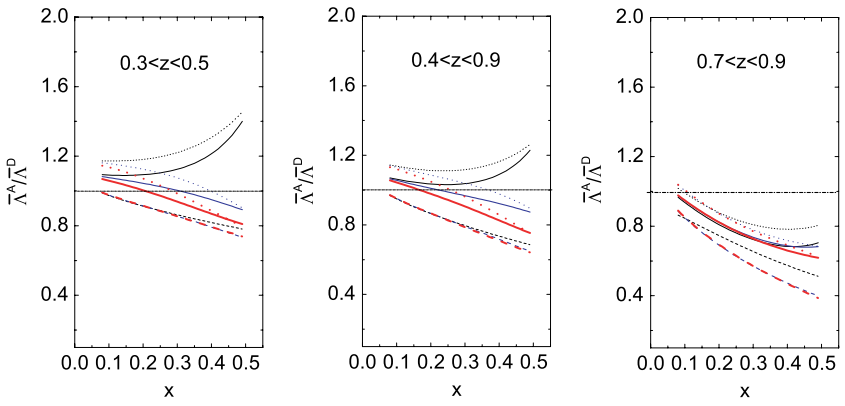

FIG. 14. (Color online) The production ratio of $\bar{\Lambda}^A/\bar{\Lambda}^D$ at $Q^2 = 5$ GeV^2 with $\hat{q} = 0.25$ GeV/fm^2. The solid, dashed, and dotted curves are the predictions of the cluster model, the rescaling model, and the pion excess model, respectively. The left figure is the result in the region $0.3 < z < 0.5$, the middle is the result in the region $0.4 < z < 0.9$, and the right is the result in the region $0.7 < z < 0.9$. The thin, normal, and thick curves correspond to the three options of the unfavored fragmentation (1), (2), (3), respectively. The target nuclei assumed here is Fe.

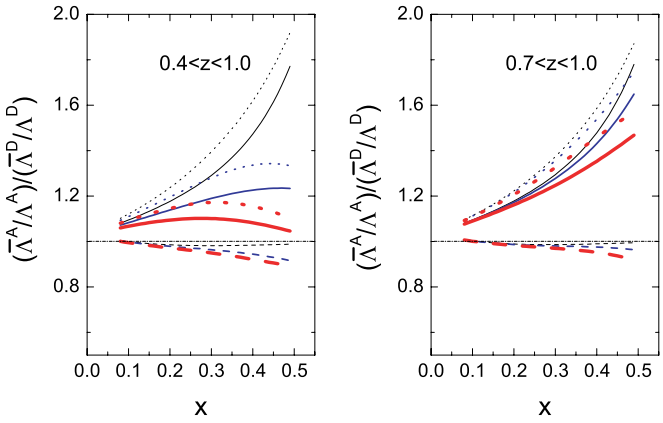

FIG. 15. (Color online) The production ratio of $(\bar{\Lambda}^A/\Lambda^A)/(\bar{\Lambda}^D/\Lambda^D)$ at $Q^2 = 5$ GeV^2 with $\hat{q} = 0.25$ GeV/fm^2, calculated in $0.7 < z < 1.0$ and $0.4 < z < 1.0$. The solid, dashed, and dotted curves are the predictions of the cluster model, the rescaling model, and the pion excess model, respectively. The thin, normal, and thick curves correspond to the three options of the fragmentation (1), (2), (3), respectively. The target nuclei assumed here is Fe.

$\bar{p}^A/p^A/\bar{p}^A/p^A$ do generate large difference with different nuclear model (Figs. 10–12). So, the ratio $(\bar{p}^A/p^A)/(\bar{p}^A/p^A)$ is another choice to check the sea content of the nuclei in experiment. Attention should be paid to extract possible background contribution as a large number of protons and antiprotons might be produced from the decays of other baryons.

$\hat{q}$ is a sensitive parameter that could largely affect the modification of fragmentation function and is not determined clearly yet. We also calculate Λ^A/Λ^D, $\bar{\Lambda}^A/\bar{\Lambda}^D$ and $(\bar{\Lambda}^A/\Lambda^A)/(\bar{\Lambda}^D/\Lambda^D)$ when $\hat{q} = 0.25$ GeV/fm^2 (Figs. 13–15). From the figures we can conclude that Λ^A/Λ^D and $\bar{\Lambda}^A/\bar{\Lambda}^D$ are largely affected by different $\hat{q}$, while $(\bar{\Lambda}^A/\Lambda^A)/(\bar{\Lambda}^D/\Lambda^D)$ is almost $\hat{q}$ independent. And $(\bar{p}^A/p^A)/(\bar{p}^A/p^A)$ also has such properties (Figs. 11 and 12). So, the ratio $(\bar{\Lambda}^A/\Lambda^A)/(\bar{\Lambda}^D/\Lambda^D)$ and $(\bar{p}^A/p^A)/(\bar{p}^A/p^A)$ are not sensitive to $\hat{q}$.

Besides, we should mention that the fixed order calculation used here is not appropriate to describe hadron production at high z where large logarithms need to be resumed. Therefore we should consider the results here as qualitative predictions rather than quantitative ones. For more convinced quantitative predictions, we would need better constrained fits of the nuclear parton distributions, rather than the earlier EMC model results adopted in this paper.

V. SUMMARY

In this paper, we adopted three models of the nuclear EMC effect: the cluster model, the rescaling model and the pion excess model, to calculate their predictions on the hadron production ratio in charged lepton semi-inclusive deep-inelastic scattering off nuclei in the large z region. Our purpose is to find hadrons which are produced mainly from the sea quarks of nucleus, so that we can distinguish between different predictions on the sea content of the nuclei. For completeness, we considered the production ratios of π^{+A}/π^{+D}, π^{-A}/π^{-D}, K^{+A}/K^{+D}, K^{-A}/K^{-D}, Λ^A/Λ^D, $\bar{\Lambda}^A/\bar{\Lambda}^D$, $(\bar{\Lambda}^A/\Lambda^A)/(\bar{\Lambda}^D/\Lambda^D)$, $(\bar{p}^A/p^A)/(\bar{p}^A/p^A)$ and found that the ratios of $(\bar{\Lambda}^A/\Lambda^A)/(\bar{\Lambda}^D/\Lambda^D)$ and $(\bar{p}^A/p^A)/(\bar{p}^A/p^A)$ are ideal to figure out the sea content of the nuclei.

More significantly, $(\bar{\Lambda}^A/\Lambda^A)/(\bar{\Lambda}^D/\Lambda^D)$ and $(\bar{p}^A/p^A)/(\bar{p}^A/p^A)$ are accessible in experiment and the behaviors of $(\bar{\Lambda}^A/\Lambda^A)/(\bar{\Lambda}^D/\Lambda^D)$ and $(\bar{p}^A/p^A)/(\bar{p}^A/p^A)$ are different for different models. According to Figs. 9 and 12, we conclude that the various models about the EMC effect with different sea behaviors can be distinguished by the future data of the x-dependence of $(\bar{\Lambda}^A/\Lambda^A)/(\bar{\Lambda}^D/\Lambda^D)$ and $(\bar{p}^A/p^A)/(\bar{p}^A/p^A)$ in semi-inclusive deep inelastic scattering process. The difference between the pion excess model and cluster model is not good enough to be checked out in experiment, but whether the sea quark is enhanced or not is clear to be distinguished according to the result.

ACKNOWLEDGMENTS

This work is partially supported by National Natural Science Foundation of China (Nos. 10421503, 10575003, 10528510), by the Key Grant Project of Chinese Ministry of Education (No. 305001), and by the Research Fund for the Doctoral Program of Higher Education (China).

[1] J. J. Aubert *et al.*, Phys. Lett. **B105**, 322 (1982).
[2] CERN NA2/EMC, J. J. Aubert *et al.*, Phys. Lett. **B123**, 275 (1983).
[3] E139, R. G. Arnold *et al.*, Phys. Rev. Lett. **52**, 727 (1984).
[4] C. H. Llewellyn Smith, Phys. Lett. **B128**, 107 (1983).
[5] M. Ericson and A. W. Thomas, Phys. Lett. **B128**, 112 (1983).
[6] R. L Jaffe, Phys. Rev. Lett. **50**, 228 (1983).
[7] C. E Carlson and T. J. Havens, Phys. Rev. Lett. **51**, 261 (1983).
[8] H. J. Pirner and J. P. Vary, Phys. Rev. Lett. **46**, 1376 (1981).
[9] F. E. Close, R. G. Roberts, and G. C. Ross, Phys. Lett. **B129**, 346 (1983).
[10] R. L. Jaffe *et al.*, Phys. Lett. **B134**, 449 (1984).
[11] F. E. Close, R. L. Jaffe, R. G. Roberts, and G. G. Ross, Phys. Rev. D **31**, 1004 (1985).
[12] O. Nachtmann and H. J. Pirner, Z. Phys. C **21**, 277 (1984).
[13] D. M. Alde *et al.*, Phys. Rev. Lett. **64**, 2479 (1990).
[14] M. A. Vasiliev *et al.*, Phys. Rev. Lett. **83**, 2304 (1999).
[15] M. B. Johnson *et al.*, Phys. Rev. Lett. **86**, 4483 (2001).
[16] G. T. Garvey and J. C. Peng, Phys. Rev. Lett. **90**, 092302 (2003).
[17] A. Airapetian *et al.* (HERMES Collaboration), Phys. Lett. **B577**, 37 (2003).
[18] H. L. Lai *et al.*, Eur. Phys. J. C **12**, 375 (2000).
[19] E. L. Berger, F. Coester, and R. B Wiringa, Phys. Rev. D **29**, 398 (1983).

[20] P. J. Sutton, A. D. Martin, R. G. Roberts, and W. J. Stirling, Phys. Rev. D **45**, 2349 (1992).
[21] O. Biebel, P. Nason, and B. R. Webbler, hep-ph/0109282.
[22] S. Kretzer, Phys. Rev. D **62**, 054001 (2000).
[23] B.-Q. Ma, I. Schmidt, and J.-J. Yang, Phys. Lett. **B574**, 35 (2003); **B547**, 245 (2002) .
[24] B.-Q. Ma, I. Schmidt, and J.-J. Yang, Phys. Lett. **B477**, 107 (2000).
[25] A. Bialas and T. Chmaj, Phys. Lett. **B133**, 241 (1983); A. Bialas and M. Gyulassy, Nucl. Phys. **B291**, 793 (1987) .
[26] E. Wang and X. N. Wang, Phys. Rev. Lett. **89**, 162301 (2002).
[27] X. Guo and X. N. Wang, Phys. Rev. Lett. **85**, 3591 (2000); X. N. Wang and X. Guo, Nucl. Phys. **A696**, 788 (2001);J. A. Osborne, E. Wang, and X. N. Wang, Phys. Rev. D **67**, 094022 (2003).
[28] B. Kopeliovich, J. Nemchik, and E. Predazzi, nucl-th/9607036.
[29] A. Accardi and H. J. Pirner, Nucl. Phys. **A711**, 264 (2002).
[30] X. N. Wang, Z. Huang, and I. Sarcevic, Phys. Rev. Lett. **77**, 231 (1996).
[31] F. Arleo, Eur. Phys. J. C **30**, 213 (2003).
[32] F. Arleo, J. High Energy Phys. 11 (2002) 044.